Evaluation of the AMPS Boundary Layer Simulations on the Ross Ice Shelf with Tower Observations

JONATHAN D. WILLE,[a] DAVID H. BROMWICH,[a,b] MELISSA A. NIGRO,[c] JOHN J. CASSANO,[c,d] MARIAN MATELING,[e,f] MATTHEW A. LAZZARA,[e,g] AND SHENG-HUNG WANG[a]

[a] *Polar Meteorology Group, Byrd Polar and Climate Research Center, The Ohio State University, Columbus, Ohio*
[b] *Atmospheric Sciences Program, Department of Geography, The Ohio State University, Columbus, Ohio*
[c] *Cooperative Institute for Research in Environmental Sciences, University of Colorado Boulder, Boulder, Colorado*
[d] *Department of Atmospheric and Oceanic Sciences, University of Colorado Boulder, Boulder, Colorado*
[e] *Antarctic Meteorological Research Center, Space Science and Engineering Center, University of Wisconsin–Madison, Madison, Wisconsin*
[f] *Department of Atmospheric and Oceanic Sciences, University of Wisconsin–Madison, Madison, Wisconsin*
[g] *Department of Physical Sciences, School of Arts and Sciences, Madison Area Technical College, Madison, Wisconsin*

(Manuscript received 8 January 2016, in final form 9 August 2016)

ABSTRACT

Flight operations in Antarctica rely on accurate weather forecasts aided by the numerical predictions primarily produced by the Antarctic Mesoscale Prediction System (AMPS) that employs the polar version of the Weather Research and Forecasting (Polar WRF) Model. To improve the performance of the model's Mellor–Yamada–Janjić (MYJ) planetary boundary layer (PBL) scheme, this study examines 1.5 yr of meteorological data provided by the 30-m Alexander Tall Tower! (ATT) automatic weather station on the western Ross Ice Shelf from March 2011 to July 2012. Processed ATT observations at 10-min intervals from the multiple observational levels are compared with the 5-km-resolution AMPS forecasts run daily at 0000 and 1200 UTC. The ATT comparison shows that AMPS has fundamental issues with moisture and handling stability as a function of wind speed. AMPS has a 10-percentage-point (i.e., RH unit) relative humidity dry bias year-round that is highest when katabatic winds from the Byrd and Mulock Glaciers exceed 15 m s^{-1}. This is likely due to nonlocal effects such as errors in the moisture content of the katabatic flow and AMPS not parameterizing the sublimation from blowing snow. AMPS consistently overestimates the wind speed at the ATT by 1–2 m s^{-1}, in agreement with previous studies that attribute the high wind speed bias to the MYJ scheme. This leads to reduced stability in the simulated PBL, thus affecting the model's ability to properly simulate the transfer of heat and momentum throughout the PBL.

1. Introduction

Forecast models rely on complex and relatively dense networks of meteorological observing stations for both data input and model testing. The surface observing network in Antarctica remains the sparsest in the world, especially with regard to vertical measurements like radiosondes and towers. Therefore, studying and comparing the modeled and observed planetary boundary layer (PBL) is a difficult activity in this region. The surface area of Antarctica is greater than that of the United States of America, yet it only has approximately 10 radiosonde sites as compared with the 69 in the contiguous United States. The limited observational network is an essential component for the production of forecasts that support the safety and operations of the U.S. Antarctic Program (USAP). These forecasts currently rely on the Antarctic Mesoscale Prediction System (AMPS; Powers et al. 2012), which employs the polar version of the Weather Research and Forecasting (Polar WRF) Model that is developed and maintained by the Polar Meteorology Group at the Byrd Polar and Climate Research Center (Bromwich et al. 2013). The AMPS forecasts are utilized by the Space and Naval Warfare Systems Center (SPAWAR), which issues all weather forecasts for the USAP. The Antarctic-specific model in AMPS provides guidance to forecasters to reduce the

Byrd Polar and Climate Research Center Contribution 1546.

Corresponding author address: David H. Bromwich, 1090 Carmack Rd. 108 Scott Hall, Columbus, OH 43210.
E-mail: bromwich.1@osu.edu

DOI: 10.1175/JAMC-D-16-0032.1

occurrence of costly flight turnarounds in the international Christchurch (New Zealand)–McMurdo (Antarctica) route and has proven to be essential for rescue missions, especially during narrow flight windows in winter. This study aims eventually to improve Antarctic boundary layer weather prediction by analyzing 1.5 yr of data provided by the 30-m-high Alexander Tall Tower! (ATT) automatic weather station on the western Ross Ice Shelf to test the performance of AMPS within the PBL with regard to local stability and the advection of moisture.

Previous AMPS verification studies have focused either on radiosondes and dropsondes or on automatic weather stations (AWSs) that take observations at a single level (Bromwich et al. 2005; Fogt and Bromwich 2008; Vázquez Becerra and Grejner-Brzezinska 2013; Russell et al. 2014). Radiosonde and dropsonde projects provide valuable information at coarse temporal resolution and throughout the troposphere with high vertical resolution. The recent "Concordiasi" field program provided 640 upper-air observations that were later utilized in AMPS testing, and the Integrated Global Radiosonde Archive provides a much larger amount of upper-air observations for model testing (Bromwich et al. 2013; Russell et al. 2014). AWSs provide long records of single-level data at high temporal resolution (typically 10-min intervals), but their low observational height (about 3 m) limits their usefulness in depicting boundary layer behavior. Steinhoff et al. (2009) observed that the Mellor–Yamada–Janjić (MYJ; Janjić 1994) PBL scheme in AMPS using the polar-modified fifth-generation Pennsylvania State University–National Center for Atmospheric Research Mesoscale Model (Polar MM5) misrepresented the surface stability as a function of wind speed at multiple AWS sites when a Ross Ice Shelf airstream was present, which is defined as a low-level topographically forced wind regime influenced by the pressure field associated with synoptic-scale cyclones over the Ross Sea. The results from that study motivated this further exploration of the AMPS boundary layer stability by using the multiple vertical levels of the ATT. While investigating model stability at the ATT, questions arose concerning the accuracy of the forecast moisture in AMPS. The moisture bias at the ATT site was evident enough to warrant further exploration in this study.

Modeling the boundary layer over Antarctica presents some unique challenges that require changes to physics parameters within models that are usually developed for midlatitude and tropical climates. Given the barrenness over ice sheets and sea ice, the zero-plane displacement is nearly zero, meaning surface winds are minimally impacted by friction. This creates smaller roughness lengths, which increases the magnitude of wind speeds over the ice while decreasing the height of the boundary layer (King and Turner 1997). Katabatic winds draining off the Transantarctic Mountains can lead to sustained winds of greater than $20\,\mathrm{m\,s^{-1}}$ on the Ross Ice Shelf that quickly mix a stable PBL. The ease with which the Antarctic boundary layer mixes makes it difficult for models to predict transitions between stable and neutral conditions. Many large-scale models traditionally applied in the midlatitudes use overly diffusive boundary layers in stably stratified regions like Antarctica that result in PBLs that underestimate turning of the wind, have greater thicknesses, and underestimate the magnitude of the nocturnal jet and the low-level-jet frequency (Holtslag et al. 2013). Previous studies have shown that models are overvigorous with mixing in the stable boundary layer and suggest that reducing the surface drag would create more realistic stability values (Holtslag et al. 2013). Keeping the mixing high in models helps to prevent the output from going into an unphysical decoupled mode, a model abnormality in which turbulent transport between the atmosphere and surface ceases, leaving the net radiation to balance the ground heat flux. Over cool surfaces with little turbulence such as the Ross Ice Shelf, a decoupled mode can lead to runaway cooling near the ground (Holtslag et al. 2013; Sterk et al. 2013).

AMPS in this study employs the MYJ local closure scheme along with the Rapid Radiative Transfer Model for global applications (RRTMG) and the Unified Noah Land Surface Model (LSM; Antarctic Mesoscale Prediction System 2015). The MYJ PBL scheme consistently overestimates near-surface wind speeds, which may affect how Polar WRF resolves stability changes (Hines and Bromwich 2008; Tastula et al. 2012; Valkonen et al. 2014). Tastula et al. (2012) found a 2.4°C warm bias over Antarctic sea ice during May (austral autumn), and Hines and Bromwich (2008) found a 2.8°C warm bias over the Greenland ice sheet during December (boreal winter). In Hines and Bromwich (2008), however, the MYJ PBL scheme along with the WRF single-moment 5-class scheme (WSM5) for microphysics had the lowest biases in 2-m temperature when compared with the Yonsei University (YSU) PBL scheme simulations. Bromwich et al. (2013) tested Polar WRF over Antarctica using the MYJ PBL; when combined with the RRTMG radiation scheme, Polar WRF, version 3.2.1, recorded mean temperature and wind speed biases of −1.3°C and $+1.4\,\mathrm{m\,s^{-1}}$ in January and +1.7°C and $+2.1\,\mathrm{m\,s^{-1}}$ in July. Bromwich et al. (2013) also tested Polar WRF using the MYJ PBL with various radiation schemes to study the Antarctic shortcomings of longwave and shortwave radiation in the Polar WRF, version 3.1.1. A shortage of clouds in the model creates a deficit in downwelling longwave radiation that correlates with a positive downwelling shortwave

radiation bias. This result indicates that the Polar WRF cloud fraction is too low, the clouds are too optically thin, or both. Testing various PBL schemes in a more convective boundary layer over the United States showed that the MYJ scheme exhibits higher positive specific humidity biases and cold temperature bias in the lower boundary layer when compared with the asymmetric convective model, version 2 (ACM2), and YSU PBL schemes (Hu et al. 2010). Above the boundary layer, MYJ has a warm temperature bias and a negative specific humidity bias, indicating weaker entrainment in the MYJ PBL scheme.

Valkonen et al. (2014) tested the Polar WRF against observations on the drifting ice breaker Research Vessel (RV) Polarstern in the Weddell Sea in the austral summer from 28 November 2004 to 2 January 2005. The study used the YSU PBL scheme, but it did test the RRTMG longwave radiation scheme used in Polar WRF. The RRTMG radiation scheme had a $-1.0°C$ surface temperature cold bias and a $+0.4\,m\,s^{-1}$ 10-m wind speed bias, similar to the summer results of Bromwich et al. (2013). The RRTMG radiation also underestimated both the downwelling and upwelling longwave radiation. The net longwave radiation bias was $-18.4\,W\,m^{-2}$ with a 0.33 correlation coefficient,and RRTMG performed worse than the RRTM longwave radiation scheme. The RRTMG radiation scheme produced a 2.0°C near-surface cold bias and an unrealistically stable boundary layer according to a radiosonde analysis. These studies indicate a possible systematic cold bias related to the RRTMG radiation scheme, at least during the summer months. In addition there is a consistent downwelling longwave radiation negative bias related to a shortage of model cloud cover.

With regard to moisture in AMPS, previous studies examined the AMPS forecast moisture values with radiosonde data after 12+ hours of prediction from model initial conditions that had assimilated prior radiosonde data. The radiosonde studies at McMurdo station show high correlation in AMPS relative humidity around 700 hPa. Around the 850-hPa level, AMPS has an approximately 10% moist bias. The positive relative humidity bias continues up to ~250 hPa with AMPS showing a weaker vertical decrease in moisture (Fogt and Bromwich 2008). An examination of precipitable water vapor from McMurdo radiosonde data reveals that AMPS is relatively accurate at simulating the precipitable water amounts, with only a 0.4-mm positive bias (Vázquez Becerra and Grejner-Brzezinska 2013). A broader view of Antarctic radiosonde data shows that AMPS generally has a moist bias at 500 hPa. Accurately simulating moisture in Antarctica is a daunting task because small variations in moisture content in extremely dry air have large impacts on moisture parameters. A $0.01\,g\,kg^{-1}$ change in water vapor mixing ratio at 500 hPa leads to a 5°C change in dewpoint when the air temperature is close to −40°C (Bromwich et al. 2005).

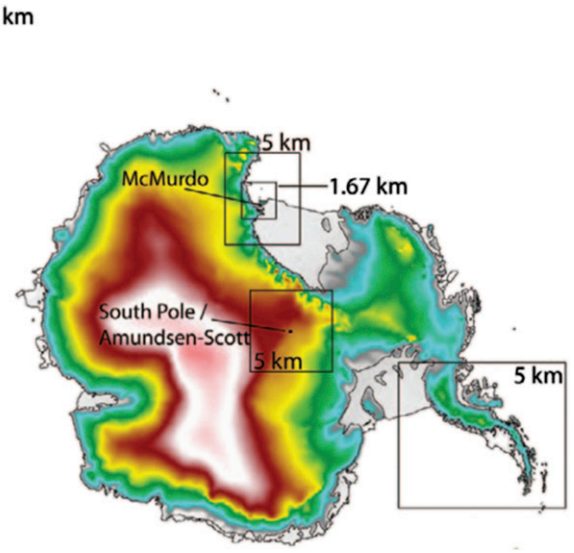

FIG. 1. AMPS model grids during the ATT analysis of 2011–12, showing 15-km (Southern Ocean), 5-km (western Ross Sea, South Pole, and Antarctic Peninsula), and 1.67-km (Ross Island area) grids. Colors represent elevation above sea level (from Powers et al. 2012).

2. AMPS

AMPS is a real-time numerical weather prediction system developed by the Polar Meteorology Group and the National Center for Atmospheric Research (NCAR) that employs Polar WRF on varying-resolution grids to generate numerical guidance utilized by numerous groups with operations in Antarctica. AMPS run at NCAR provides a 120-h forecast two times per day using the National Centers for Environmental Prediction Global Forecasting System initial conditions and regional three-dimensional variational data assimilation (3D-Var; Barker et al. 2004). At the time of the ATT study in 2011–12, AMPS had a 15-km continent-scale domain along with smaller higher-resolution domains, as seen in Fig. 1. Figure 2 provides a closer look at the coverage of AMPS domain 3 along with the approximate location of the ATT. This study utilized 5-km (157 × 190 grid points) domain-3 AMPS data containing 43 sigma levels run daily at 0000 and 1200 UTC. There is the option to use domain-5 AMPS data, which have a horizontal resolution of 1.67 km because the ATT is within that domain (Fig. 2). Because the ATT site is two grid points away from the domain boundary, however, domain-3 data were used to avoid any issues with the tower's proximity to the model's relaxation zone. The first 12 h of each model run are not used in this study, and the subsequent

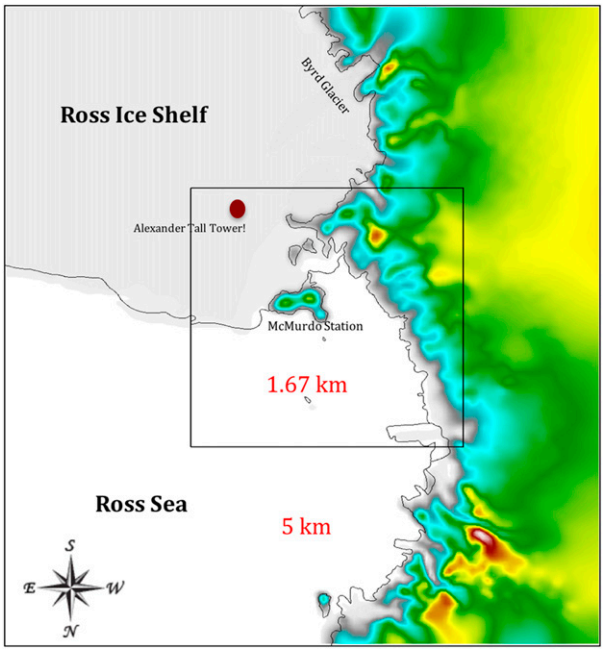

FIG. 2. The AMPS–ATT analysis utilizes AMPS 5-km domain 3 as displayed here. The interior square is AMPS 1.67-km domain 5, and the red dot is the approximate location of the ATT. The proximity of the ATT to the relaxation boundary of domain 5 raises concerns as to model accuracy, and therefore domain 5 is not considered in this study. Colors represent AMPS elevation above sea level, not including any ice shelves. The domain resolutions are valid for 1 Nov 2008–31 Dec 2012. The figure is rotated 180° from Fig. 1.

12–23 forecast hours are concatenated to create a continuous hourly forecast record. Previous studies indicate that polar models require at least 8 h of spinup for PBL conditions like the katabatic flow and temperature to become quasi steady (Parish and Waight 1987; Parish and Cassano 2003). Polar MM5 and Polar WRF testing over Greenland selected a 12-h spinup (Cassano et al. 2001; Hines and Bromwich 2008), and so this study utilized a 12-h spinup for consistency in results.

The AMPS archive at NCAR contains full model forecast output as WRF native-format data. The Polar Meteorology Group houses a smaller archive that contains basic model output variables (at http://polarmet.osu.edu/AMPS/). Both NCAR and the Polar Meteorology Group work on model verification and research to continually improve the accuracy of the AMPS model, which is the motivation for this project. AMPS data utilized here come from the Earth System Grid data portal (https://www.earthsystemgrid.org/project/amps.html).

3. Polar WRF

Polar WRF contains various optimizations for polar environments. These modifications primarily encompass the land surface model, including optimal values of snow thermal properties and improved heat flux calculations. Time-variable fractional sea ice is represented by separate calls to the surface-layer scheme for ice and open water, and the surface heat fluxes are areally averaged to obtain the final values for the fractional sea ice grid box. Polar WRF also has adjustments to the thermal and radiative properties of ice and snow surfaces that have been shown to improve AMPS forecast performance (Powers 2009). The modified models have been assessed in the Arctic and Antarctic (Hines and Bromwich 2008; Powers 2009; Bromwich et al. 2009, 2013; Hines et al. 2011, 2015; Cassano et al. 2011). Polar code has been merged into recent versions of the official WRF releases.

The WSM5 (Hong et al. 2004) parameterization for cloud physics is altered to have the diagnostic relation for ice number concentration depend on ice mass content instead of on temperature (Hines and Bromwich 2008). AMPS simulates shortwave radiation with the Goddard shortwave scheme with 11 spectral bands that depict both diffuse and direct solar radiation (Chou and Suarez 1994), which accurately represents the diurnal cycle over an ice surface (Hines and Bromwich 2008). At the time of the study, AMPS still used the MYJ local closure scheme. The MYJ PBL scheme has prognostic turbulent kinetic energy along with an eta surface-layer scheme that is based on similarity theory and a nonsingular implementation of level-2.5 Mellor–Yamada closure for turbulence in the PBL and free atmosphere (Janjić 1994). Surface physics is handled by the four-layer Noah LSM (Tewari et al. 2004; Bromwich et al. 2009; Hines et al. 2015). The Noah LSM has a Penman–Monteith equation for evapotranspiration that includes sublimation so as to account for sublimation from frozen surfaces (Bromwich et al. 2009).

At the beginning of the study period from 1 March to 27 April 2011, AMPS ran WRF, version 3.0.1.1, which utilized the RRTM longwave radiation scheme. For the remainder of the ATT study period (May 2011–August 2012), AMPS used the upgraded WRF, version 3.2.1, that changed the longwave radiation scheme to RRTMG. During the time between versions 3.0.1.1, and 3.2.1 of WRF, the snow albedo formula was upgraded. The rest of the WRF physics options, such as the Goddard shortwave radiation scheme, the Monin–Obukhov (Janjić eta) surface-layer scheme, the Unified Noah LSM, and the WSM5 microphysics scheme, remained constant throughout the study period.

4. Alexander Tall Tower!

The Alexander Tall Tower! was installed approximately 160 km south of McMurdo station on the Ross

FIG. 3. Photograph of the ATT taken during the 2015/16 field season (provided through the courtesy of Carol Costanza).

Ice Shelf during the 2010/11 USAP field season for a joint project with the University of Wisconsin–Madison and the University of Colorado Boulder (Lazzara et al. 2011, 2012). The tower provides multiple levels of temperature, relative humidity, wind speed, wind direction, and single-level pressure along with net longwave and shortwave radiation measurements at 10-s intervals (Fig. 3). The ATT instrument heights and manufacturer stated accuracy are listed in Table 1. The data are manually quality controlled and processed to 10-min averages by the Antarctic Meteorological Research Center (AMRC) in Madison, Wisconsin, as outlined in Lazzara et al. (2012). Like other automatic weather stations maintained by the AMRC, the temperature data are manually checked after going through an automated process to account for possible observational errors caused by direct and/or diffuse solar radiation in low wind speeds and frost deposition. The wind speed and direction are manually analyzed to account for "frozen wind instruments" errors that are evident if the station reports wind speeds of zero or a constant wind direction for longer than 1 day.

The AMPS data were linearly interpolated both horizontally and vertically to match the tower location and the tower instrumentation heights. The lowest levels of the 5-km AMPS terrain-following coordinates provide data at approximately 12 and 42 m above the surface, and so model skin temperature is included to increase data resolution. The skin temperature is derived from the surface energy balance of the Noah LSM. The model-interpolated 2-m temperature is excluded from the dataset because of strong warm biases found during the beginning of the project. ATT data from March 2011 to August 2012 are incorporated into the analysis. In the figures containing vertical averages, the AMPS hourly forecasts and the corresponding nonmissing ATT observations (matching values only) are each averaged for the (mostly) colder March–August (MAMJJA) and warmer September–February (SONDJF) periods from 2011 to 2012 to create two averages of equal population members. For the stability-transition plots, scatterplots, wind roses, and histograms in the results, MAMJJA 2011 and MAMJJA 2012 are combined to increase the data counts. MAMJJA 2011 and MAMJJA 2012 qualitatively have the same results throughout the analysis, and therefore combining the two datasets simply creates clearer findings. Because AMPS increased the Polar WRF horizontal resolution during January of 2013, a second set of SONDJF data from 2012 to 2013 was not utilized for the study. The error bars are the standard deviation of the mean ($\mathrm{sd}/n^{1/2}$), where sd is the standard deviation and n is the number of observations.

The Alexander Tall Tower! is one of a few towers on the Antarctic continent used to monitor atmospheric boundary layer conditions. One study that analyzed PBL data on the Antarctic Plateau from a 45-m

TABLE 1. ATT instrument, heights, and manufacturer-stated accuracy (Nigro et al. 2016, manuscript submitted to *Wea. Forecasting*).

Instrument	Height (m)	Manufacturer-stated accuracy
R. M. Young Co. platinum resistance temperature	0.85, 1.83, 3.75, 7.25, 14.75, and 29.75	±0.3°C
Vaisala, Inc., HMP45C-L humidity	7.25 and 29.75	±2.0%
R. M. Young Wind Sentry cup anemometer	1.34	$\pm 0.5\ \mathrm{m\ s^{-1}}$
R. M. Young aerovanes	3.75, 7.25, 14.75, and 29.75	$\pm 0.3\ \mathrm{m\ s^{-1}}$
Vaisala pressure	2.3	—
Campbell Scientific, Inc., acoustic depth gauge	3.2	—
Kipp and Zonen B.V. CNR2-L net longwave and shortwave radiation	29.75	—

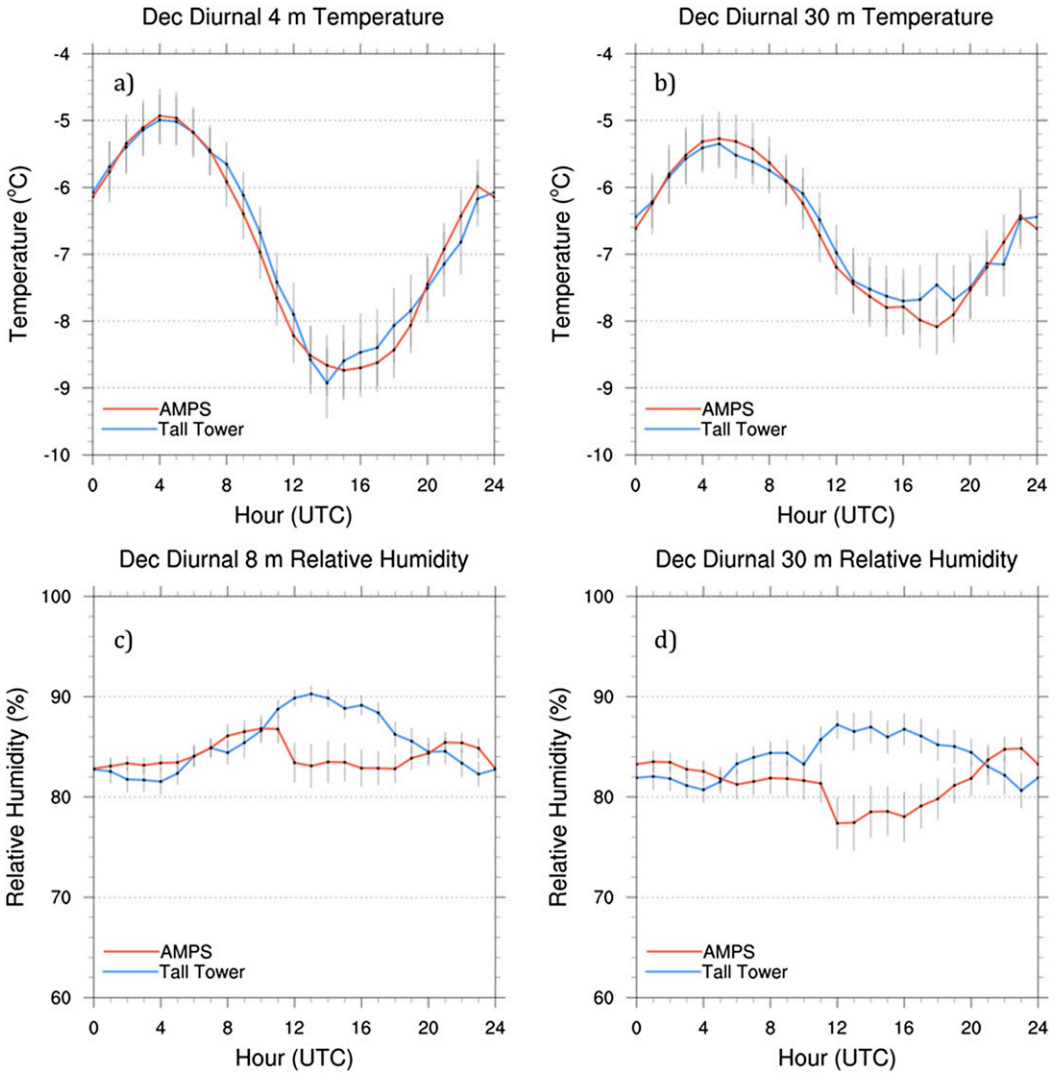

FIG. 4. Average December 2011 (a) 4- and (b) 30-m diurnal temperature and (c) 8- and (d) 30-m diurnal relative humidity for AMPS and the ATT. The error bars represent the standard error of the mean. UTC is 11 h ahead of local time.

meteorological tower at Dome C station from 2009 to 2010 encountered problems with accurate moisture measurements because of frost deposition, most notably during winter (Genthon et al. 2013). The air sampled by the moisture sensors on the ATT may not be representative of free air because excess moisture above supersaturation may be deposited on the instruments before being sampled by the sensors (Genthon et al. 2013). This would result in a dry bias when air with high moisture content is being measured. The ATT is located in a warmer climate than the Dome C tower but is still subject to measurement errors resulting from extreme cold. The ATT uses a Campbell Scientific, Inc., HMP45C-L probe to measure relative humidity. The HMP45C-L specifications state that the accurate temperature measurement range is from −39.2° to +60°C for relative humidity. Because the ATT occasionally measures temperatures of approximately −50°C during the winter months, this range of accuracy brings some observed humidity values into question. Nonetheless, because the model biases shown below are similar for all seasons and the average winter temperature remains 10°–20°C warmer than the lowest temperature for accurate measurement, there is confidence in the relative humidity measurements during winter.

5. Results

a. Diurnal cycle

The multiple levels of temperature measurement at the tower provide information on the diurnal cycle as a

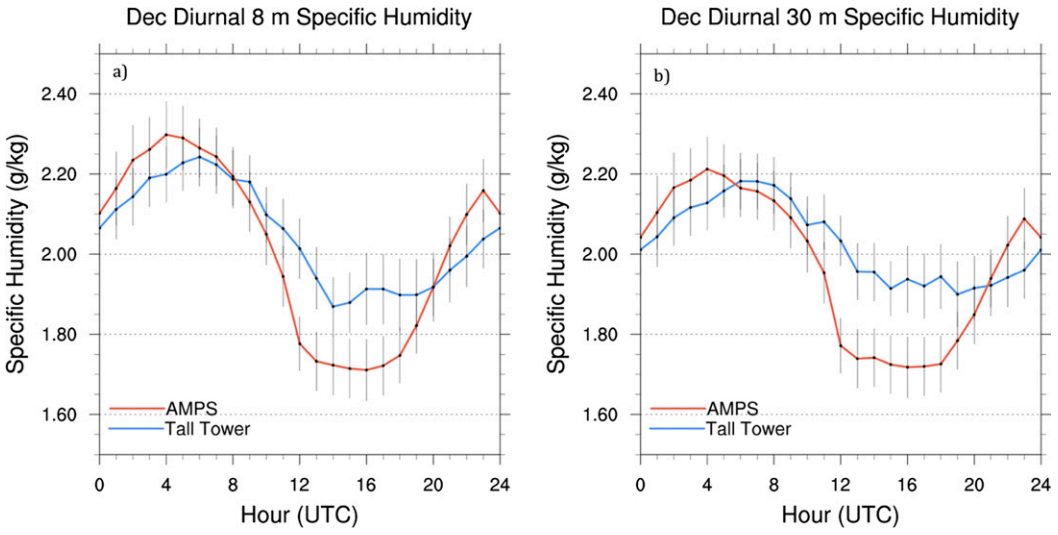

FIG. 5. As in Fig. 4, but for (a) 4- and (b) 30-m diurnal specific humidity.

function of height above the surface, as opposed to the situation with previous AWS stations that only provide one level of data. This added vertical information shows that AMPS accurately captures the dampening of the diurnal cycle with height during December, as seen in Fig. 4. According to the Student's *t* test, the differences between AMPS and the ATT diurnal cycle are statistically insignificant for both the 4- and 30-m temperatures for every hour of the day, and the standard error shows that the temperature variance of the December diurnal cycle is small when compared with a winter month. This result helps to confirm that the vertical interpolation in AMPS is accurate at heights just above the surface in summer boundary layer conditions. Although the temperature is accurately simulated, AMPS has a significant dry bias during the night (1200–1900 UTC) when the sun is lower in the sky. The relative humidity (relative to water) dry bias increases with height: the maximum relative humidity dry bias increases by 4 percentage points (i.e., 4 RH units) at 30 m relative to 8 m (Fig. 4). Using *p* values, the AMPS and observed 30-m relative humidities are statistically similar during the afternoon but become statistically different at night. The specific humidity in AMPS and ATT follows a diurnal cycle that is similar to that of temperature. Like the AMPS relative humidity, the specific humidity between 1200 and 1900 UTC is underestimated at 4 and 30 m and amplifies with height, highlighting the AMPS dry bias during the summer night (Fig. 5). Between 1100 and 1200 UTC, the AMPS relative humidity drops by 5 percentage points. The specific humidity decreases at a faster rate between these hours as well. This coincides with the point at which the 23rd forecast hour from the 1200 UTC model run from the previous day switches over to the 12th forecast hour in the 0000 UTC run. To determine whether this drop in moisture is physically realistic or is a model artifact, the diurnal cycle plots were recreated using the 12–36 forecast hours from the earlier 1200 UTC model run. The plots for the 12–36 forecast hours show a slight dampening of the drop in AMPS relative humidity, as the dry bias is 3 percentage points smaller during the night hours at 30 m (not shown), indicating some artificiality: note, however, that there is no evidence in Figs. 4a and 4b of a discontinuity in the temperature.

The errors in the AMPS diurnal relative humidity are still evident in August during which month the sun is always below the horizon. The winter dry bias increases with height as the 30-m dry bias ranges from 10 to 13 percentage points for all hours while the 8-m dry bias ranges from 7 to 10 percentage points (Fig. 6). The specific humidity confirms that the dry bias in AMPS increases with height. The 8-m specific humidity bias ranges from 0.02 to 0.06 g kg^{-1} while the 30-m specific humidity dry bias ranges from 0.05 to 0.09 g kg^{-1} bias in AMPS (not shown). Without solar radiation, there is no diurnal temperature cycle as the average temperature remains constant during all hours. The temperature becomes dependent on external forcing, causing large variance in the hourly temperature over the course of August. According to the Student's *t* test, the AMPS and ATT 8- and 30-m diurnal temperatures are mostly statistically indistinguishable for every hour. The boundary layer during August is more stably stratified, which leads to more nonlinear vertical temperature profiles. This introduces some error in the analysis because the AMPS temperature is linearly interpolated. A recent analysis of the Alexander Tall Tower! data in Nigro et al. (2016, manuscript submitted to *Wea. Forecasting*), however,

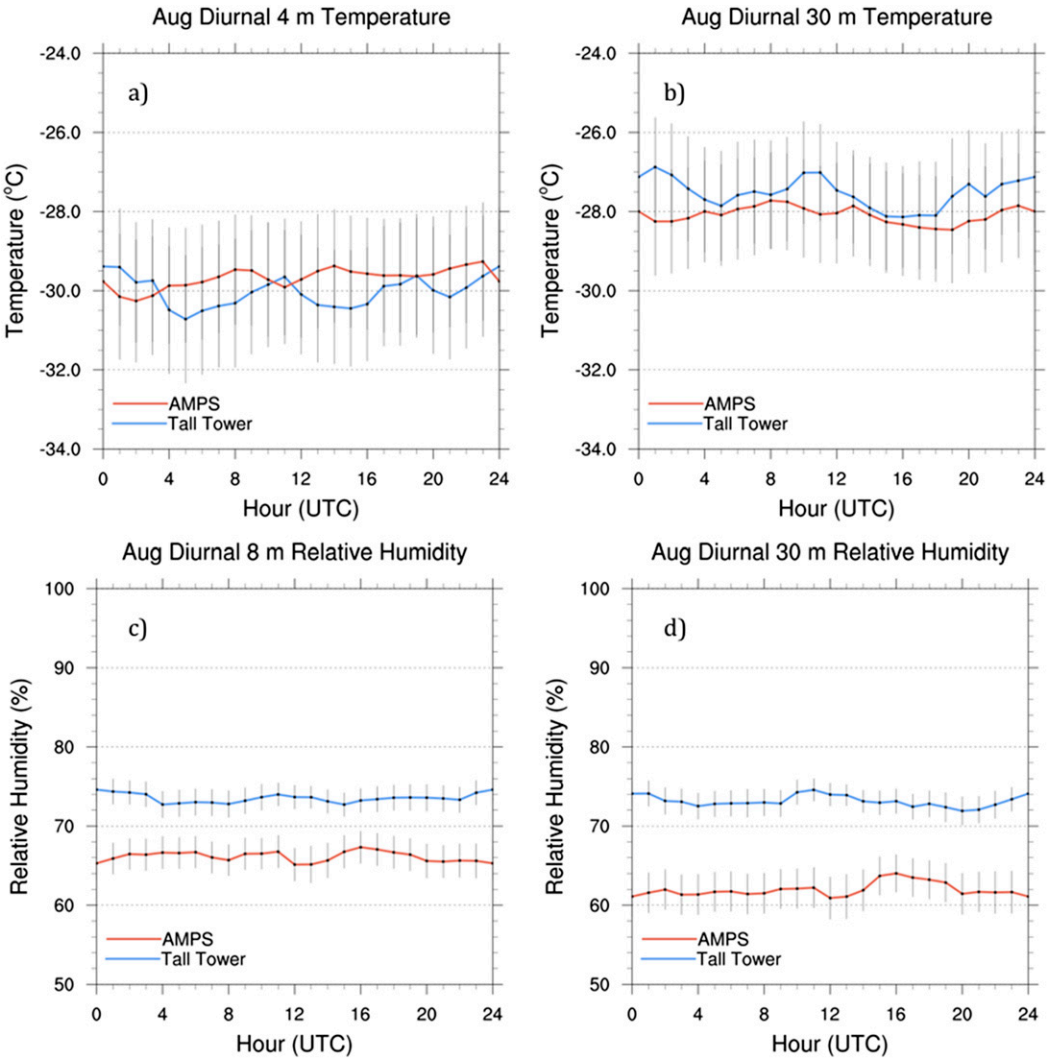

FIG. 6. As in Fig. 4, but for August 2011.

shows that very stably stratified profiles account for only 3.7% of all PBL profiles during a 2-yr period, likely because of the strong katabatic flow and the resultant vertical mixing, and therefore errors from the AMPS linear interpolation are infrequent.

From October to March when the diurnal cycle is evident, nighttime dry biases in AMPS appear in every month except November (not shown). January could not be analyzed because of instrumentation errors. In addition, each month from October to March had a 10° southward wind direction bias in AMPS (not shown). The wind speeds generally remained within the range of standard error for every month in the study period (not shown).

b. *ATT synthesis*

The continuous hourly measurements from the ATT over a multiyear period allow for an extended examination of the AMPS lower PBL. The annual data are divided into two seasons: the average of MAMJJA approximates winter conditions, and the SONDJF average represents summer. Figure 7 displays the vertical structure of relative humidity and wind speed in AMPS and the ATT observations in MAMJJA and SONDJF without filtering for special conditions. The temperature and wind direction are within the range of standard error (not shown), but statistically significant errors appear in the AMPS MAMJJA wind speed and MAMJJA and SONDJF relative humidity according to the Student's *t* test. Figure 7a shows a 1–2 m s^{-1} model overestimation in wind speeds for MAMJJA, but Fig. 7b shows an accurate depiction of the SONDJF wind speed. AMPS also has a 5–10-percentage-point dry bias during MAMJJA relative to the 8- and 30-m relative humidity measurements on the ATT. The model dry bias is still

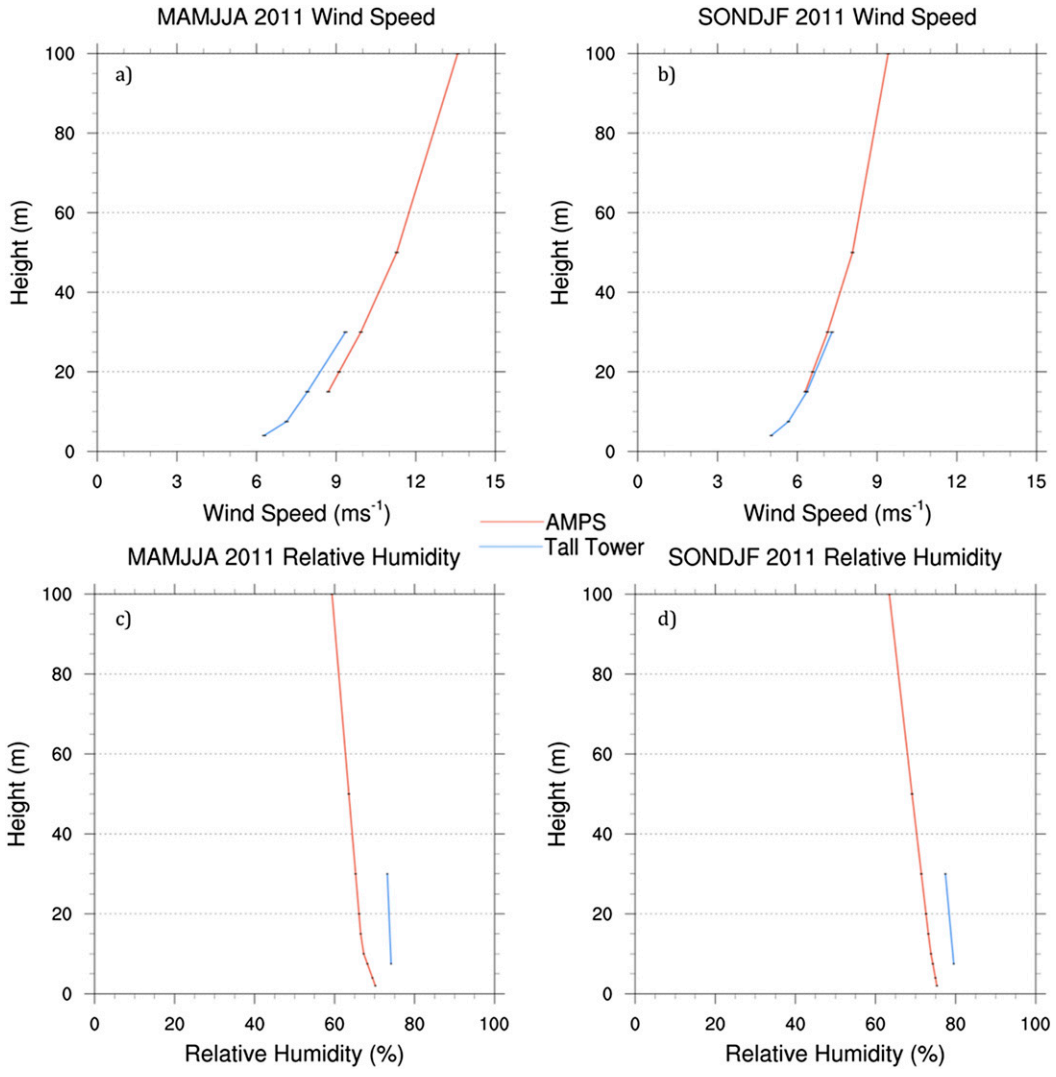

FIG. 7. Average vertical structure of (a),(b) wind speed and (c),(d) relative humidity at the ATT site averaged over (left) MAMJJA 2011 and (right) SONDJF 2011/12. The error bars represent the standard error of the mean.

evident during SONDJF but is less pronounced, with AMPS showing a 5-percentage-point dry bias. On a seasonal basis, AMPS has higher accuracy during the warmer months as the overall relative humidity increases and there is a lower frequency of strongly stable conditions that are more challenging to simulate (Cassano et al. 2016).

Because the structure of the temperature inversion is strongly dependent on near-surface wind conditions, examining AMPS performance under various wind speeds provides additional insight into the model PBL dynamics. In this study, an inversion refers to an increase in temperature with height. Figure 8 breaks down the average vertical profiles into different wind speed regimes on the basis of the 15-m observed and 15-m simulated wind speed averaged over a period of 1 h. If AMPS and the ATT both show an hourly wind speed within one of the three wind speed categories (0–5, 5–15, or $>15\,\mathrm{m\,s^{-1}}$), the temperature and relative humidity from that time step are included in the analysis. During the light-wind conditions ($0–5\,\mathrm{m\,s^{-1}}$) and the stronger-wind conditions ($>15\,\mathrm{m\,s^{-1}}$) in the MAMJJA period, the model has an ~1°C cold bias on average in the lowest 10 m AGL. During the SONDJF period, only during the light-wind conditions is there a 1°C cold bias; the other wind speed categories are within the range of standard error (not shown). We suggest that this cold bias in light-wind conditions during SONDJF is tied to the model skin temperature and limited turbulent mixing. During both the MAMJJA and SONDJF periods, the AMPS

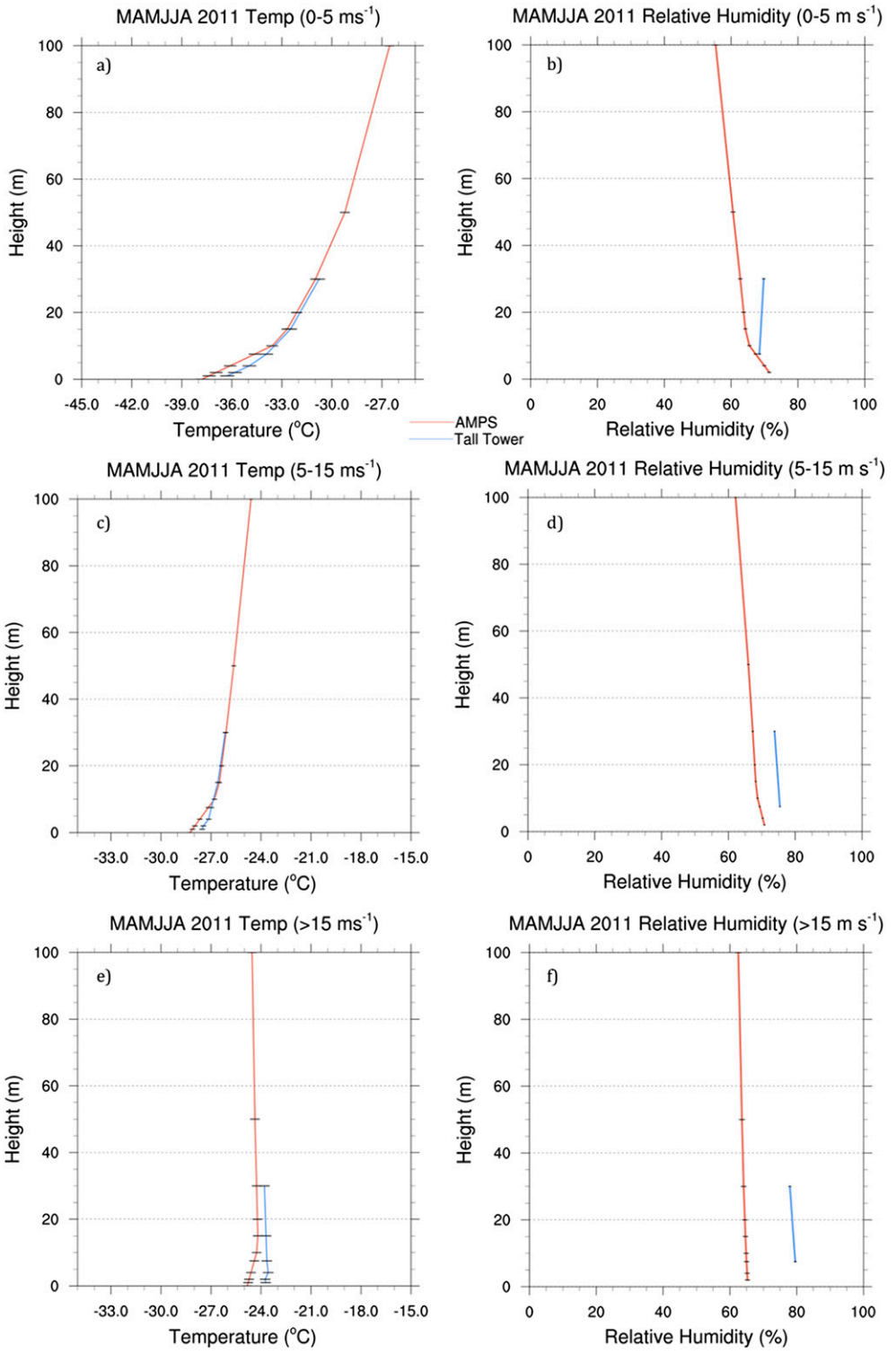

FIG. 8. Average vertical structure of (left) temperature and (right) relative humidity at the ATT site when model and observed 15-m wind speeds are (a),(b) less than 5 m s^{-1}, (c),(d) between 5 and 15 m s^{-1}, and (e),(f) greater than 15 m s^{-1}. The profiles are averaged over MAMJJA 2011. The error bars represent the standard error of the mean.

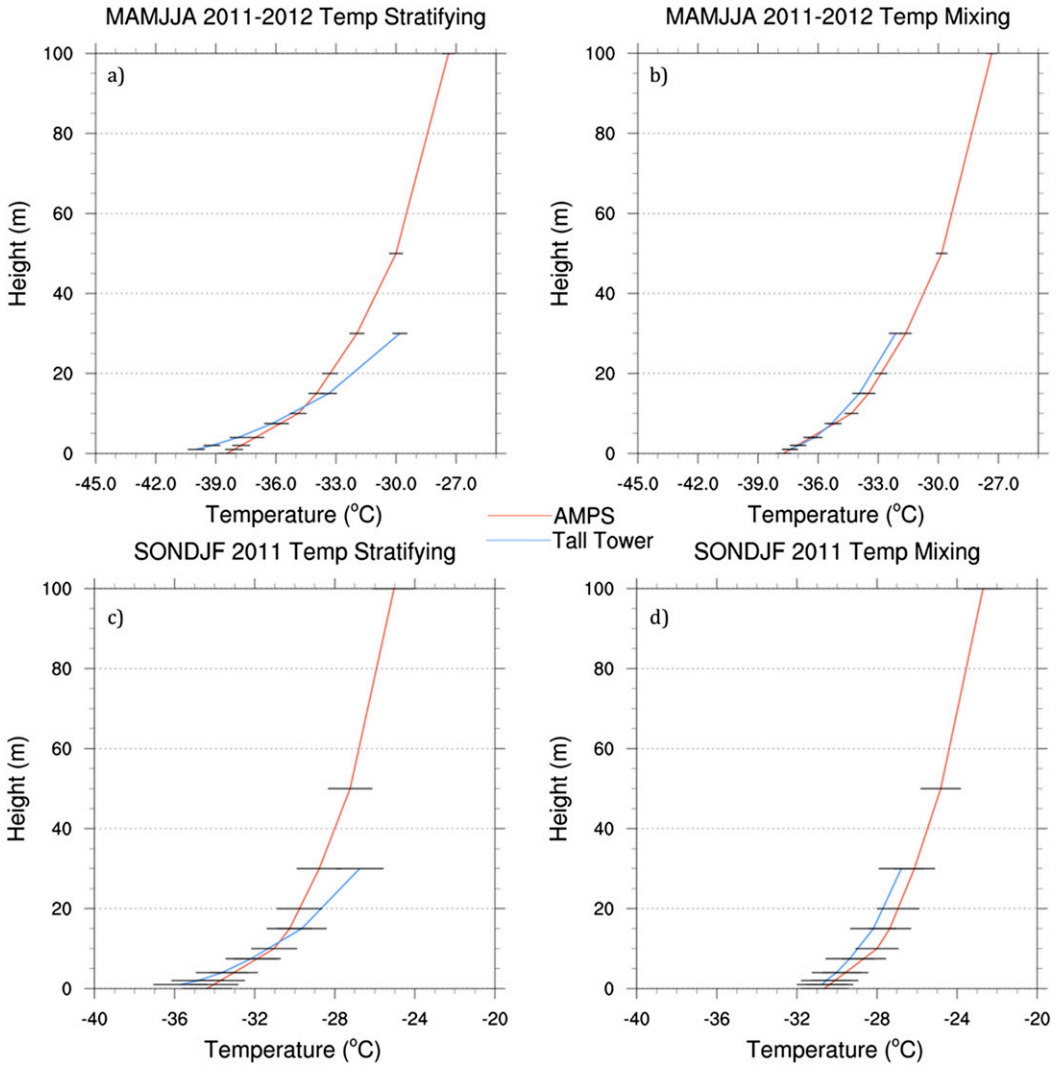

FIG. 9. Average vertical structure of temperature at the ATT site when model and observed PBL conditions are (left) stratifying and (right) mixing out during the (a),(b) combined MAMJJA 2011 and MAMJJA 2012 and (c),(d) SONDJF 2011/12 periods. Stratifying (mixing) events are defined as the inversion strength (30 − 1 m) increasing (decreasing) by 3°C or more during a 1-h period for both AMPS and observations. The error bars represent the standard error of the mean.

relative humidity errors increase as the wind speeds increase. As seen in Fig. 8b, the AMPS relative humidity in MAMJJA for light winds (0–5 m s^{-1}) agrees with the ATT 15-m relative humidity and has a 5-percentage-point dry bias at 30 m. Once the winds are greater than 15 m s^{-1}, however, the model dry bias increases to 15 percentage points (i.e., 15 RH units) at all levels. The observational average relative humidity increases from 70% for light winds to 80% for stronger winds. Relative humidity normally increases in high winds because of the increased sublimation from the ice surface and the blowing snow. The Noah LSM accounts for sublimation from the surface, but sublimation from blowing snow is not a model parameter. The observed and simulated relative humidities increase slightly with speeds of greater than 15 m s^{-1} during SONDJF, with a less pronounced dry bias than MAMJJA (not shown).

c. *Stability transitions*

Steinhoff et al. (2009) showed that AMPS struggled at simulating changes in stability. Figures 9 and 10 examine the structure of the PBL during stability transitions. Here we define stability changes as an hourly increase or decrease in inversion strength (30 − 1 m) that is greater than or equal to 3°C. When the inversion strength is increasing it is classified as stratifying, and when the inversion strength is decreasing it is classified as mixing. Data from MAMJJA 2011 and MAMJJA 2012 are

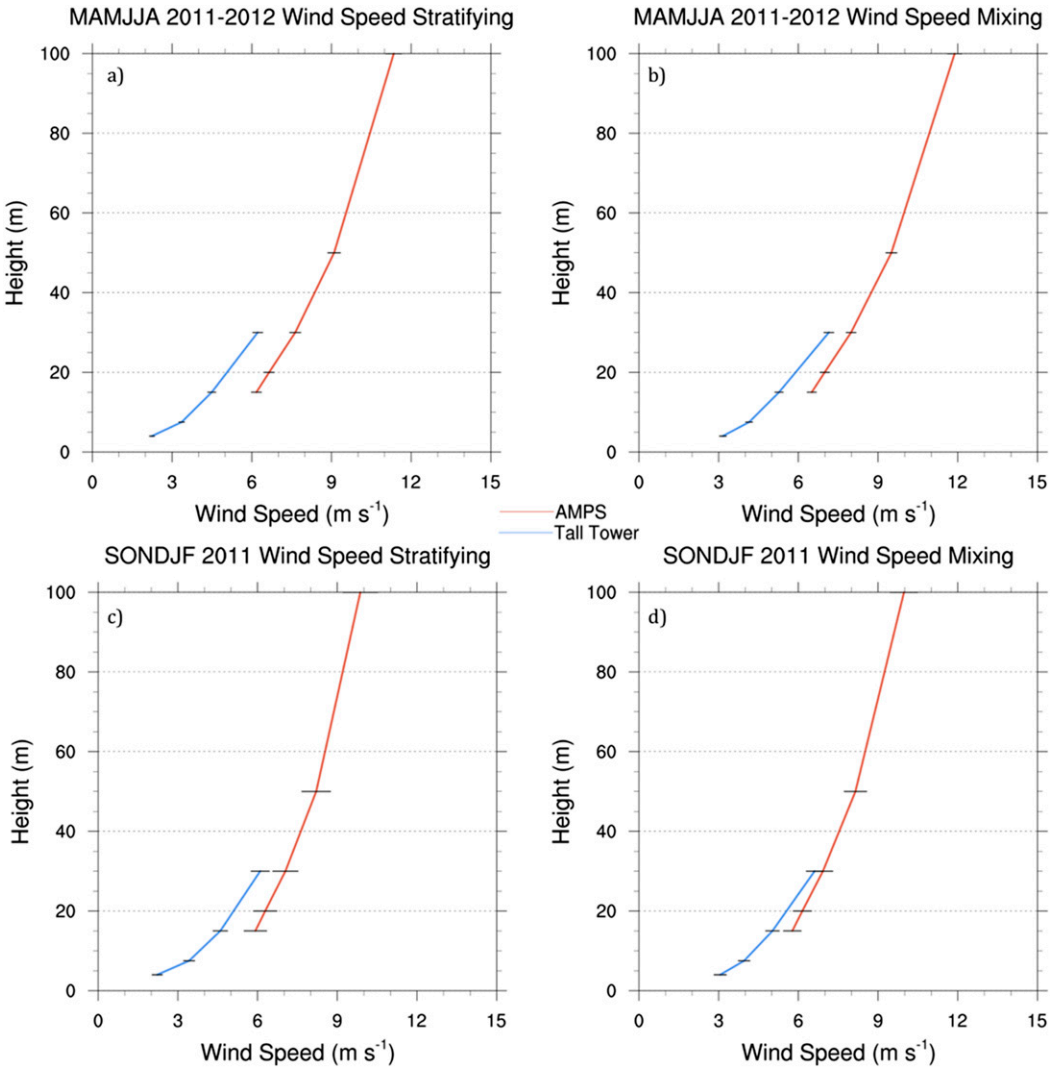

FIG. 10. As in Fig. 9, but for wind speed.

combined to decrease the standard error for the analysis. During mixing events, for both MAMJJA and SONDJF there is good temperature agreement between AMPS and observations. However, during stratifying events, the model has a cold bias around the 30-m level during both seasons, with MAMJJA showing a 3°C cold bias. During MAMJJA, the model has a statistically significant 1°C warm bias at the surface according to the Student's *t* test (Fig. 9a). These biases result in AMPS underestimating the inversion strength when stratification is occurring, perhaps because of a lag in the Noah LSM.

The AMPS dry bias is equally evident during stratifying and mixing events with an ~10-percentage-point dry bias during winter and summer with no discernable differences in observed relative humidity in the two stability regimes (not shown). Wind speeds are overestimated in both stability-change regimes regardless of season aside from SONDJF mixing, for which model errors are within the range of standard error (Fig. 10). The largest model wind speed errors of $+2\,\mathrm{m\,s^{-1}}$ occur during stratifying conditions in MAMJJA. The negative inversion-strength bias in AMPS during stratifying conditions may be related to the overestimated wind speeds that transport warmer air from aloft to the surface. The inversion-strength errors could also be the result of the land surface model lagging behind the often-rapid changes in stability at the surface when the observed wind speeds decrease.

d. Relationship between wind and relative humidity

Because the AMPS relative humidity bias is greatest when the wind speed is greater than $15\,\mathrm{m\,s^{-1}}$, it is

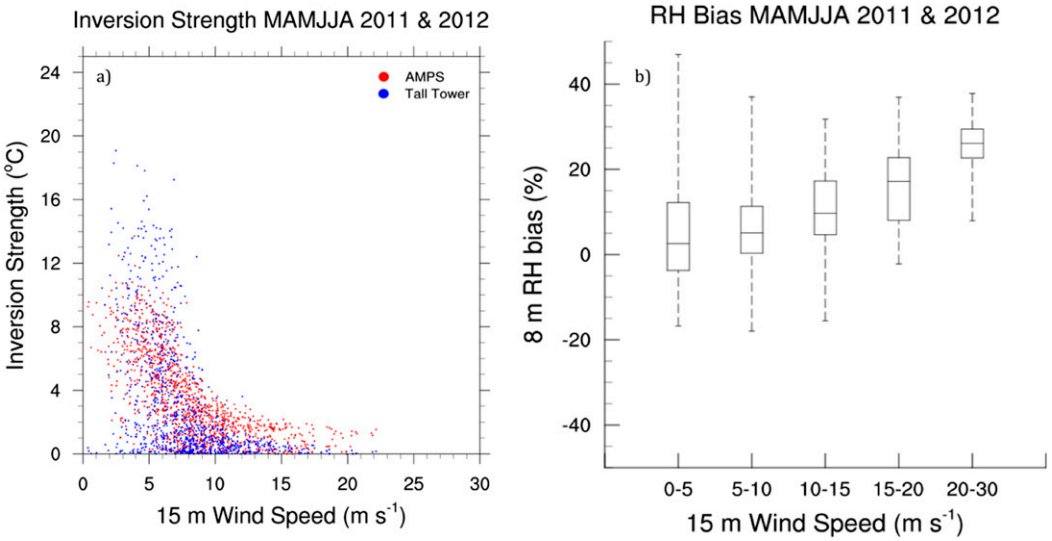

FIG. 11. The (a) inversion strength and (b) 8-m relative humidity bias of each AMPS forecast hour plotted against the corresponding 15-m wind speed ATT observation, for MAMJJA 2011 and MAMJJA 2012 combined. For (a), inversion strength is the difference between the 30- and 1-m temperatures for both AMPS and the ATT and a point is plotted only if the model and observational 15-m wind speeds are within 0.5 m s^{-1} for that particular hour. For (b), the relative humidity bias is the observed value minus the model result and there is no requirement for agreement between model and observed wind speeds for a point to be plotted. The whiskers represent the extreme values for each bin, and the boxes show the 25th-percentile, median, and 75th-percentile values.

important to determine the source of the high winds and to analyze the relationship between wind direction and relative humidity biases while assessing the accuracy of the AMPS wind direction. Figure 11b clarifies the relationship between the wind speed and the increasing relative humidity bias. While the box-and-whisker plot shows noise in the bias extremes during low winds, the overall relative humidity bias median increases to ~25 percentage points in the highest model wind speeds. The greatest differences between observed and model relative humidity occur during MAMJJA, with AMPS having discernable dry biases during all wind speeds.

An analysis of the wind direction reveals that the dominant wind regime at the ATT is katabatic winds from the southwest. There is a discrepancy in average wind direction between AMPS and the observed wind direction. According to the AMPS wind direction in Fig. 12a, winds from the southwest account for about 70% of the total flow at the ATT during MAMJJA 2011 and MAMJJA 2012. That percentage drops just below 60% when looking at the observed southwest wind direction. This slight difference between the AMPS and observed wind directions may be related to the relatively coarse 5-km model grid used during the study period. The wind rose using observed wind values shows that a greater percentage of winds come from the west (not shown). This discrepancy becomes important for the relative humidity bias as Fig. 12b shows about 95% of AMPS dry biases during high winds occur when the winds are from the southwest. Because the primary source of katabatic wind at the ATT site comes from Byrd Glacier to the southwest and the Mulock Glacier farther to the north, as visualized by the higher-resolution 1.1-km 2015 AMPS vector-averaged wind field in Fig. 13, the southward wind direction bias might imply that AMPS is overestimating the amount of katabatic drainage from Byrd Glacier (Liu and Bromwich 1993). More observations along the base of the Transantarctic Mountains are needed to further investigate this wind direction bias. During the summer months (SONDJF), winds higher than 15 m s^{-1} are still primarily from the southwest, with a few more cases from the Ross Sea direction to the north. This is expected as observed Ross Ice Shelf airstream patterns are less prevalent in the summer (Nigro and Cassano 2014).

e. *Wind speed–dependent stability*

To further explore how relative humidity and stability change with wind speed, Fig. 11a examines the inversion strength (30 − 1 m) of the individual population members used in the vertical averages through scatterplots. To remove wind speed errors from the analysis, the model and observational data at each individual hour are required to have 15-m wind speeds within 0.5 m s^{-1} of each other. The inversion strength profile in Fig. 11a shows the inversion strength decreasing as the wind

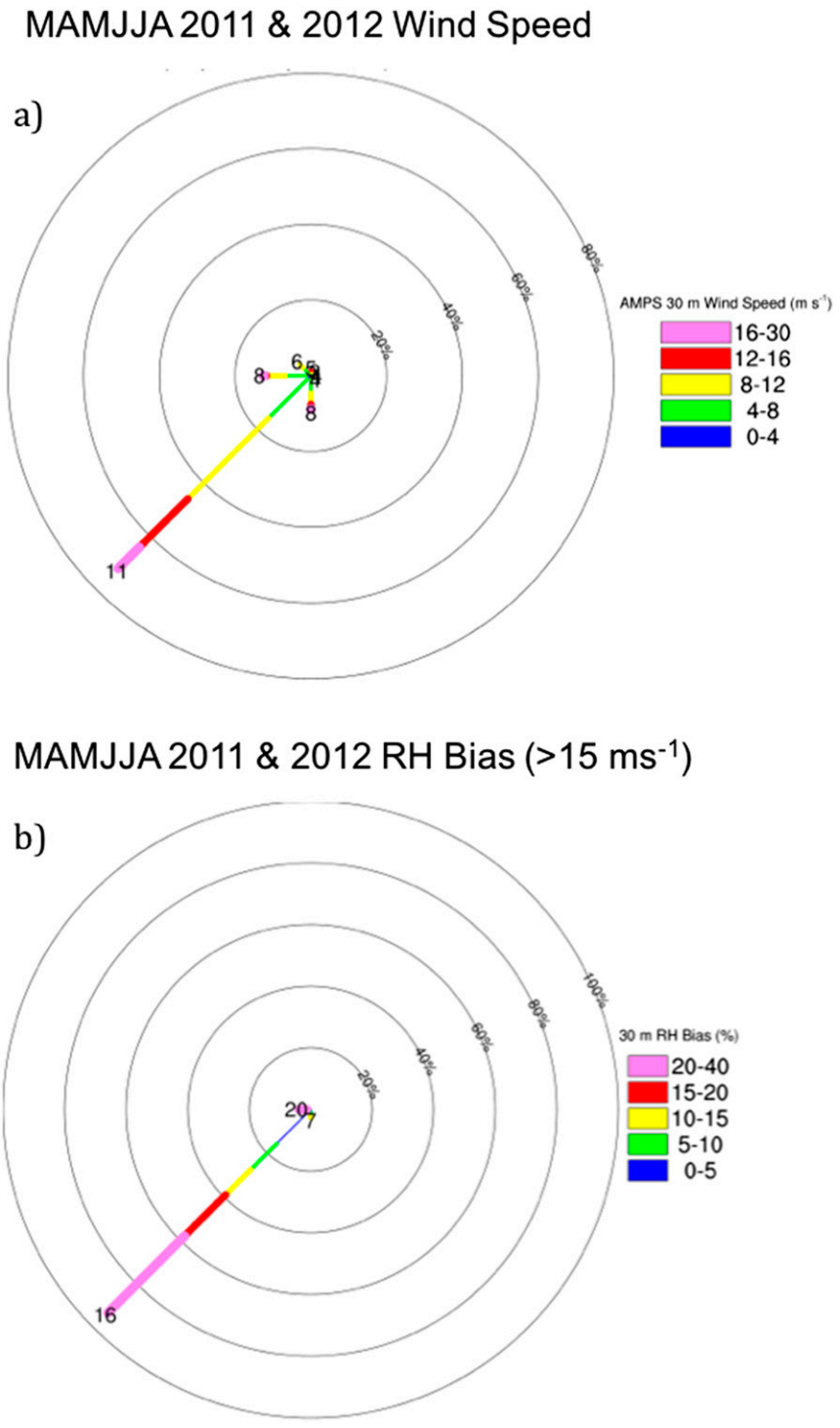

FIG. 12. An eight-petal wind rose at the ATT site according to the 30-m AMPS wind direction for (a) wind speed for all model wind speeds and (b) the relative humidity bias when model and observed 30-m wind speeds are greater than 15 m s^{-1}. The relative humidity bias in (b) is observation minus model. The numbers at the end of each petal represent average wind speed for a particular wind direction in (a) and the average relative humidity bias in (b).

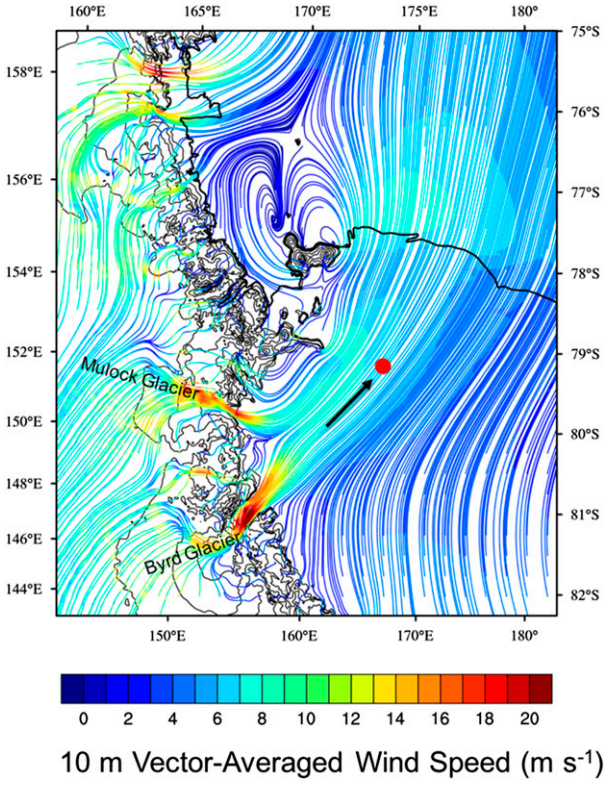

FIG. 13. The 2015 annual vector-average 10-m winds from the 1.1-km AMPS grid illustrate the topographic forcing from Mulock and Byrd Glaciers. The red dot is the location of ATT, and the arrow is parallel to the observed vector-average direction.

speeds increase. Figure 11a also shows a clear two-pronged problem in the model's handling of stability. For lower wind speeds in the MAMJJA period, AMPS is unable to capture the most intense inversions greater than 11°C. When the highest wind speeds ($>15\,m\,s^{-1}$) occur, however, the model maintains inversions of around 2°C even though the observations show isothermal conditions. AMPS displays the same underestimation of the inversion strength for slower wind speeds and overestimation of the inversion strength for faster wind speeds during SONDJF, but with smaller error magnitudes. The transition between underestimating and overestimating inversion strengths occurs around the 4–8 $m\,s^{-1}$ range, which is nearly the same wind speed range described in Riordan (1977) when examining the threshold for PBL stability changes using data from a tower at Plateau station despite much colder conditions at this station located at 3624 m above sea level on the East Antarctic Plateau.

Histograms are a useful method to quantify the wind speed–inversion-strength relationship shown in the scatterplot. Figures 14 and 15 examine the differences between AMPS and ATT inversion strengths when both perceive the wind speed to be between certain ranges (i.e., essentially subtracting the dots in Fig. 11a). Figure 14 examines the instances in which the AMPS inversion strength exceeds the ATT inversion strength for MAMJJA (positive bias), and Fig. 15 covers the instances in which the ATT inversion strength exceeds AMPS for MAMJJA (negative bias). In the positive-bias plot, the largest inversion-strength differences (>8°C) occur when the winds are weaker than 6 $m\,s^{-1}$. This cold bias in lighter-wind conditions is tied to the model skin temperature and may in part be the result of the model entering a decoupled mode, leading to runaway surface cooling for near-calm conditions. Conditions in which AMPS overestimates the inversion strength by more than 4°C when the wind speed is between 0 and 4 $m\,s^{-1}$ only account for about 5% of the total model positive inversion biases for MAMJJA and SONDJF, however.

During MAMJJA, the number of positive biases reaches a maximum at 6–8 $m\,s^{-1}$, accounting for 22% of positive-bias occurrences. As the winds increase past the 6–8 $m\,s^{-1}$ range, the frequency of biases decreases to 5% of positive biases in the 14–16 $m\,s^{-1}$ range (Fig. 14). This alludes to a model-physics mixing error that is allowing AMPS to generate weak inversions despite high wind speeds. For SONDJF the positive biases reach a maximum at 4–6 $m\,s^{-1}$ but then decrease past 6–8 $m\,s^{-1}$ until essentially disappearing at 14–16 $m\,s^{-1}$ (not shown).

The negative biases (i.e., when the ATT inversion strength exceeds AMPS) reach a maximum number of occurrences at the 4–6 $m\,s^{-1}$ range for both MAMJJA and SONDJF. The highest negative inversion-strength biases (<−4°C) occur at the 4–6 $m\,s^{-1}$ range for both time periods, accounting for 31% of all negative biases during MAMJJA (Fig. 15). In essence, around the 4–8 $m\,s^{-1}$ range, AMPS makes a transition from underestimating PBL stability to overestimating stability. Steinhoff et al. (2009) observed that AMPS using Polar MM5 together with the MYJ scheme generated anomalously strong inversions when winds were between 6 and 8 $m\,s^{-1}$, which matches the observations made in the histograms (Polar WRF together with the MYJ scheme).

The inversion-strength–wind speed relationship is less well defined during SONDJF, but a general decrease in inversion strength with increasing wind speed is evident (not shown). This verifies that AMPS has difficulty properly capturing changes in stability when winds are around 6 $m\,s^{-1}$ on the Ross Ice Shelf. Also, when one examines cases in which the simulated and observed wind speeds are in reasonable agreement, AMPS has more of a tendency to overestimate than to underestimate the static stability. As discussed earlier

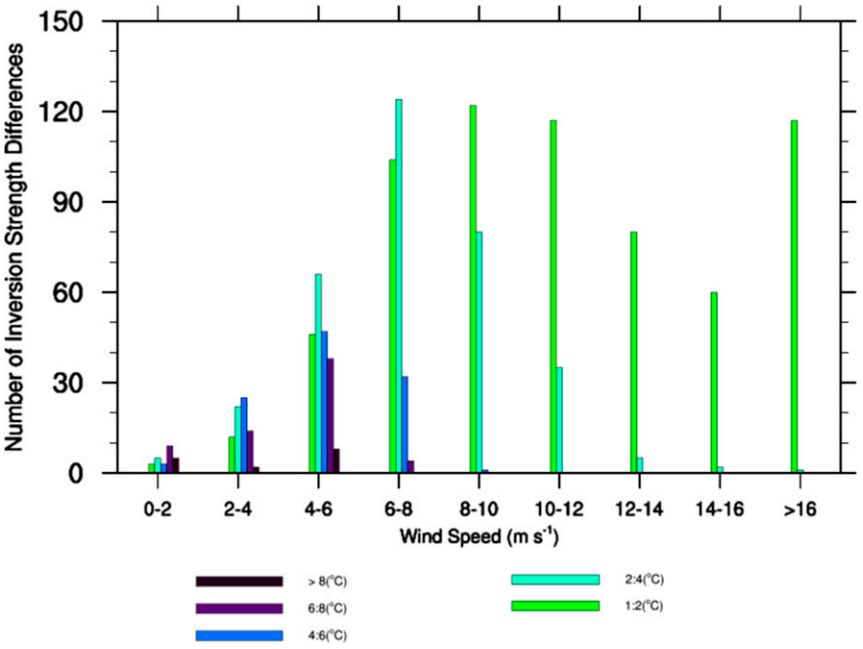

FIG. 14. Histogram of the positive AMPS inversion-strength biases vs 15-m wind speed for the MAMJJA 2011 and 2012 combined periods. Data points are selected if both model and observational wind speeds fall between a given wind speed range. Within each wind speed range, the inversion-strength difference is calculated and then assigned to a given inversion-strength-difference range. Inversion-strength biases between 0° and 1°C are not included.

though, the high wind speed bias leads to excessive mixing in the AMPS PBL.

6. Discussion

From the diurnal ATT results, AMPS is very capable of capturing the dampening of the diurnal temperature cycle with height, despite limited vertical levels near the surface. The average vertical profiles show AMPS matching the temperature, wind speed, and wind direction during SONDJF. During times when the ATT records mixing conditions, AMPS accurately predicts temperature and wind speed, especially during SONDJF. This is likely aided by the general overestimation of near-surface winds in AMPS.

The most troublesome variables throughout the study are relative humidity and the relationship between stability and wind speed. In general, it appears that AMPS overestimates the wind speed, which agrees with previous examinations of the Polar WRF that attribute these errors to the MYJ scheme (Hines and Bromwich 2008; Tastula et al. 2012; Bromwich et al. 2013; Valkonen et al. 2014). This study revealed that the model high wind speed bias reduces the gradient in temperature inversions during stratifying conditions and more broadly leads to errors in the relationship between wind speed and PBL stability.

The wind speed biases in AMPS are much higher during stratification conditions than during mixing conditions, which is likely diminishing the model stability as seen in Fig. 10. Comparisons against the ATT data reveal that the overestimation of wind speed in AMPS during times of stratification slows the AMPS development of the inversion in lower PBL. A previous comparison study of PBL schemes (Bromwich et al. 2013) showed that the MYJ scheme overestimates wind speeds in the Antarctic by 1–2 $m\,s^{-1}$, which is likely contributing to the underestimated PBL stability as seen in this study.

The underestimation of the stratification rate is part of a broader issue in AMPS, with the model mischaracterizing stability as a function of wind speed. Steinhoff et al. (2009) first revealed a possible problem in how AMPS handles stability as a function of wind speed when using AMPS with Polar MM5. That study displayed the MYJ PBL scheme in AMPS mishandling the inversion strength during moderate wind speeds by producing strong surface cooling despite local AWS sites that reported surface warming possibly related to PBL mixing. Hines and Bromwich (2008)

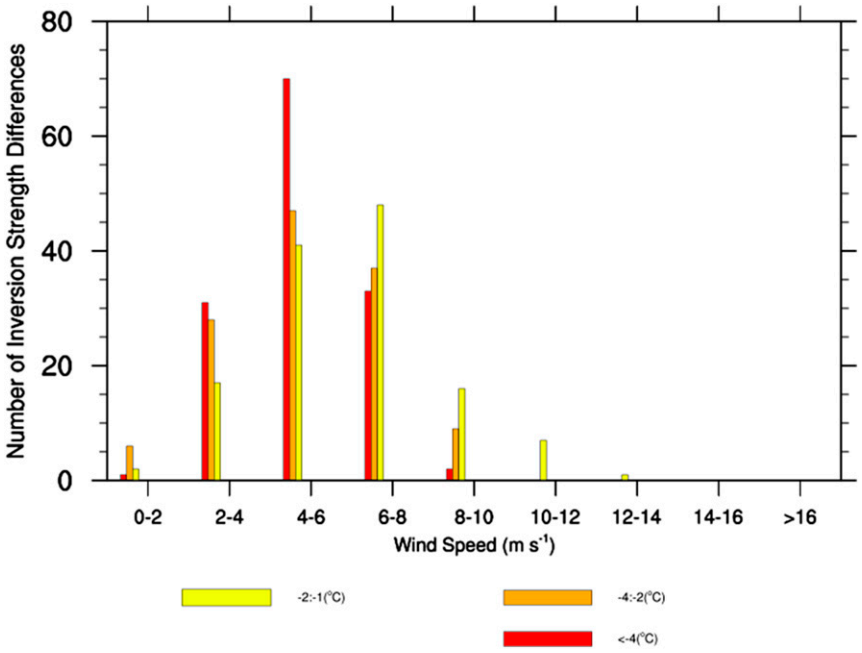

FIG. 15. As in Fig. 14, but for negative AMPS inversion strength biases and inversion-strength biases between −1° and 0°C are not included.

documented a persistent overestimation of the 10-m winds over the Greenland ice sheet when testing the MYJ scheme in Polar WRF. This wind speed overestimation from the MYJ scheme is likely reducing the stability of the AMPS PBL. The highest frequency of errors occurs when AMPS creates weak inversions in winds greater than 6 m s^{-1}, when in reality the profile is isothermal. In general, from the 12–23-forecast-hour range utilized in this study, AMPS always favored an overestimation of wind speeds rather than an underestimation.

From Riordan (1977) and this study, 4–8 m s^{-1} appears to be the wind speed threshold at which observed inversions within the PBLs begin making a transition to isothermal conditions. The scatterplots and histograms show that this wind speed range is also that for which AMPS makes the transition from underestimating PBL stability to overestimating stability. During the stability transition threshold of 4–8 m s^{-1}, there appears to be an equal frequency of AMPS underestimating and overestimating the observed inversion-strength range. This observed wind speed threshold corresponds to the thresholds defined in other studies. Using a 30-m meteorological tower over a snow-covered surface, Acevedo et al. (2016) determined that the limit wind speed at 15 m is 5.04 m s^{-1}. This study defines the crossover threshold as a point at which the average vertical gradient of turbulent kinetic energy switches signs. When below the threshold, the very stable PBL is decoupled, leading to surface cooling—especially over the Antarctic ice surface. This limits the heat flux and increases the thermal gradient throughout the PBL. Once above the threshold, the weakly stable PBL is fully vertically coupled with continuous turbulence and greater entrainment of warmer air to the surface (Acevedo et al. 2016). It is important for AMPS to correctly capture the crossover threshold to properly simulate the transfer of heat and momentum throughout the PBL.

An examination of relative humidity was not the original intent of this study, as previous work has shown that AMPS-forecast moisture parameters are generally slightly more moist when compared with radiosonde data (Bromwich et al. 2005; Fogt and Bromwich 2008; Vázquez Becerra and Grejner-Brzezinska 2013). Contrary to previous studies of moisture in Antarctica, the results from this study demonstrate a clear and consistent dry bias in AMPS at the ATT site. In diurnal terms, the AMPS dry bias is most prominent at night and increases with height. On the seasonal time scale, AMPS underestimates the relative humidity, especially for wind speeds greater than 15 m s^{-1}. During these high winds, AMPS is not parameterizing the sublimation from blowing snow, which is likely contributing to the AMPS dry bias. Given the well-documented slight positive bias of AMPS moisture

at the nearby McMurdo station and at other coastal sites in Antarctica, the local dry bias at the ATT is likely related to the advection of drier air to the ATT site and not the local impact in AMPS. The annual mean 10-m winds from the 1.1-km AMPS grid implemented after this study period to better represent the topographic forcing show that katabatic drainage from the Byrd and Mulock Glaciers to the southwest is the main wind regime at the ATT (Fig. 13). In addition, the highest relative humidity biases occur during the Ross Ice Shelf airstream when strong katabatic winds are present from the southwest (Steinhoff et al. 2009).

The diurnal plots show that the dry bias is largest at night. Since the katabatic flow is more developed at night (Monti et al. 2002), the dry bias is likely related to AMPS overestimating the magnitude of the katabatic flow through the ATT site, underestimating the moisture content of the katabatic flow from Byrd Glacier, or a combination of the two. Follow-on work using small instrumented aircraft that measure the entire depth of the PBL at the ATT site shows that the AMPS dry biases increase past the 30-m level of the ATT during summer. To explore the advection hypothesis, future AMPS studies should focus on the katabatic flow draining down Byrd Glacier and its sensitivity to regional behavior of PBL schemes. In addition, AWSs located at the top and bottom of the glacier can be compared with AMPS to determine the accuracy of the wind speed and moisture content of the katabatic wind flowing down Byrd Glacier.

Accurately predicting the wind speed in Antarctica is clearly necessary for ensuring the safety of flight operations on the ice. Properly simulating the wind speed–stability relationship is essential for an accurate depiction of vertical motion and momentum fluxes in the PBL, which influence various atmospheric processes, such as cloud development, that are important for aviation. The local dry bias observed at the ATT site also has consequences for cloud development for other regions that are significantly influenced by the katabatic wind. Because the infrastructure for model testing over Antarctica is relatively sparse, it is likely that there are other regions in Antarctica with similar dry biases that have yet to be observed.

Acknowledgments. We thank Linda Keller, David Mikolajczyk, Jonathan Thom, George Weidner, and Lee Welhouse from the University of Wisconsin–Madison for their help with the Alexander Tall Tower! AWS equipment, installation, and maintenance and also the data, which are supported by National Science Foundation (NSF) Grant ANT-1245663. The NSF via UCAR AMPS Grant GRT 0032749 to The Ohio State University and Grant ANT-1245737 to the University of Colorado Boulder funded this research.

REFERENCES

Acevedo, O. C., L. Mahrt, F. S. Puhales, F. D. Costa, L. E. Medeiros, and G. A. Degrazia, 2016: Contrasting structures between the decoupled and coupled states of the stable boundary layer. *Quart. J. Roy. Meteor. Soc.*, **142**, 693–702, doi:10.1002/qj.2693.

Antarctic Mesoscale Prediction System, 2015: Current AMPS configuration. Accessed 4 August 2015. [Available online at http://www2.mmm.ucar.edu/rt/amps/information/configuration/configuration.html.]

Barker, D. M., W. Huang, Y.-R. Guo, A. J. Bourgeois, and Q.-N. Xiao, 2004: A three-dimensional variational data assimilation system for MM5: Implementation and initial results. *Mon. Wea. Rev.*, **132**, 897–914, doi:10.1175/1520-0493(2004)132<0897:ATVDAS>2.0.CO;2.

Bromwich, D. H., A. J. Monaghan, K. W. Manning, and J. G. Powers, 2005: Real-time forecasting for the Antarctic: An evaluation of the Antarctic Mesoscale Prediction System (AMPS). *Mon. Wea. Rev.*, **133**, 579–603, doi:10.1175/MWR-2881.1.

——, K. M. Hines, and L.-S. Bai, 2009: Development and testing of Polar Weather Research and Forecasting Model: 2. Arctic Ocean. *J. Geophys. Res.*, **114**, D08122, doi:10.1029/2008JD010300.

——, F. O. Otieno, K. M. Hines, K. W. Manning, and E. Shilo, 2013: Comprehensive evaluation of Polar Weather Research and Forecasting Model performance in the Antarctic. *J. Geophys. Res. Atmos.*, **118**, 274–292, doi:10.1029/2012JD018139.

Cassano, J. J., J. E. Box, D. H. Bromwich, L. Li, and K. Steffen, 2001: Evaluation of Polar MM5 simulations of Greenland's atmospheric circulation. *J. Geophys. Res.*, **106**, 33 867–33 890, doi:10.1029/2001JD900044.

——, M. E. Higgins, and M. W. Seefeldt, 2011: Performance of the Weather Research and Forecasting Model for month-long pan-Arctic simulations. *Mon. Wea. Rev.*, **139**, 3469–3488, doi:10.1175/MWR-D-10-05065.1.

——, M. A. Nigro, and M. A. Lazzara, 2016: Characteristics of the near surface atmosphere over the Ross Ice Shelf, Antarctica. *J. Geophys. Res.*, **121**, 3339–3362, doi:10.1029/2005JD006185.

Chou, M.-D., and M. J. Suarez, 1994: Technical report series on global modeling and data assimilation. Vol. 3: An efficient thermal infrared radiation parameterization for use in general circulation models. NASA Tech. Memo. 104606, Vol. 3, 84 pp. [Available online at https://archive.org/details/nasa_techdoc_19950009331.]

Fogt, R. L., and D. H. Bromwich, 2008: Atmospheric moisture and cloud cover characteristics forecast by AMPS. *Wea. Forecasting*, **23**, 914–930, doi:10.1175/2008WAF2006100.1.

Genthon, C., D. Six, H. Gallee, P. Grigioni, and A. Pellegrini, 2013: Two years of atmospheric boundary layer observations on a 45-m tower at Dome C on the Antarctic plateau. *J. Geophys. Res. Atmos.*, **118**, 3218–3232, doi:10.1002/jgrd.50128.

Hines, K. M., and D. H. Bromwich, 2008: Development and testing of Polar Weather Research and Forecasting (WRF) Model. Part I: Greenland ice sheet meteorology. *Mon. Wea. Rev.*, **136**, 1971–1989, doi:10.1175/2007MWR2112.1.

——, ——, L.-S. Bai, M. Barlage, and A. G. Slater, 2011: Development and testing of Polar WRF. Part III: Arctic land. *J. Climate*, **24**, 26–48, doi:10.1175/2010JCLI3460.1.

——, ——, ——, C. M. Bitz, J. G. Powers, and K. W. Manning, 2015: Sea ice enhancements to Polar WRF. *Mon. Wea. Rev.*, **143**, 2363–2385, doi:10.1175/MWR-D-14-00344.1.

Holtslag, A. A. M., and Coauthors, 2013: Stable atmospheric boundary layers and diurnal cycles: Challenges for weather and climate models. *Bull. Amer. Meteor. Soc.*, **94**, 1691–1706, doi:10.1175/BAMS-D-11-00187.1.

Hong, S.-Y., J. Dudhia, and S.-H. Chen, 2004: A revised approach to ice microphysical processes for the bulk parameterization of clouds and precipitation. *Mon. Wea. Rev.*, **132**, 103–120, doi:10.1175/1520-0493(2004)132<0103:ARATIM>2.0.CO;2.

Hu, X.-M., J. W. Nielsen-Gammon, and F. Zhang, 2010: Evaluation of three planetary boundary layer schemes in the WRF Model. *J. Appl. Meteor. Climatol.*, **49**, 1831–1844, doi:10.1175/2010JAMC2432.1.

Janjić, Z. I., 1994: The step-mountain eta coordinate model: Further developments of the convection, viscous sublayer, and turbulence closure schemes. *Mon. Wea. Rev.*, **122**, 927–945, doi:10.1175/1520-0493(1994)122<0927:TSMECM>2.0.CO;2.

King, J. C., and J. Turner, 1997: *Antarctic Meteorology and Climatology*. Cambridge University Press, 290 pp.

Lazzara, M. A., J. E. Thom, L. J. Welhouse, L. M. Keller. G. A. Weidner, M. Nigro, and J. J. Cassano, 2011: USAP Antarctic Automatic Weather Station Program status and field report. *Sixth Antarctic Meteorological Observation, Modeling, and Forecasting Workshop*, Hobart, Australia, Australian Bureau of Meteorology, Paper 1.2. [Available online at http://amrc.ssec.wisc.edu/abstracts/AMOMFW2011-Lazzara-AWS-final.pdf.]

——, G. A. Weidner, L. M. Keller, J. E. Thom, and J. J. Cassano, 2012: Antarctic Automatic Weather Station program: 30 years of polar observation. *Bull. Amer. Meteor. Soc.*, **93**, 1519–1537, doi:10.1175/BAMS-D-11-00015.1.

Liu, Z., and D. H. Bromwich, 1993: Acoustic remote sensing of planetary boundary layer dynamics near Ross Island, Antarctica. *J. Appl. Meteor.*, **32**, 1867–1882, doi:10.1175/1520-0450(1993)032<1867:ARSOPB>2.0.CO;2.

Monti, P., H. J. S. Fernando, M. Princevac, W. C. Chan, T. A. Kowalewski, and E. R. Pardyjak, 2002: Observations of flow and turbulence in the nocturnal boundary layer over a slope. *J. Atmos. Sci.*, **59**, 2513–2534, doi:10.1175/1520-0469(2002)059<2513:OOFATI>2.0.CO;2.

Nigro, M. A., and J. J. Cassano, 2014: Identification of surface wind patterns over the Ross Ice Shelf, Antarctica, using self-organizing maps. *Mon. Wea. Rev.*, **142**, 2361–2378, doi:10.1175/MWR-D-13-00382.1.

Parish, T. R., and K. T. Waight III, 1987: The forcing of Antarctic katabatic winds. *Mon. Wea. Rev.*, **115**, 2214–2226, doi:10.1175/1520-0493(1987)115<2214:TFOAKW>2.0.CO;2.

——, and J. J. Cassano, 2003: The role of katabatic winds on the Antarctic surface wind regime. *Mon. Wea. Rev.*, **131**, 317–333, doi:10.1175/1520-0493(2003)131<0317:TROKWO>2.0.CO;2.

Powers, J. G., 2009: Performance of the WRF V3.1 polar modifications in an Antarctic severe wind event. Preprints, *10th WRF Users' Workshop*, Boulder, CO, NCAR. [Available online at http://www2.mmm.ucar.edu/wrf/users/workshops/WS2009/abstracts/P3B-26.pdf.]

——, K. W. Manning, D. H. Bromwich, J. J. Cassano, and A. M. Cayette, 2012: A decade of Antarctic science support through AMPS. *Bull. Amer. Meteor. Soc.*, **93**, 1699–1712, doi:10.1175/BAMS-D-11-00186.1.

Riordan, A. J., 1977: Variations of temperature and air motion in the 0- to 32-meter layer at Plateau Station, Antarctica. *Meteorological Studies at Plateau Station, Antarctica*. P. C. Dalrymple, et al., Eds., Antarctic Research Series, Vol. 25, Amer. Geophys. Union, 113–127, doi:10.1002/9781118664872.ch8.

Russell, J. O. H., D. Parsons, and S. Cavallo, 2014: An evaluation of the Antarctic Mesoscale Prediction System using unique new data from the CONCORDIASI field program. *13th Annual Student Conf.*, Atlanta, GA, Amer. Meteor. Soc. [Available online at https://ams.confex.com/ams/94Annual/webprogram/Paper242588.html.]

Steinhoff, D. F., S. Chaudhuri, and D. H. Bromwich, 2009: A case study of a Ross Ice Shelf airstream event: A new perspective. *Mon. Wea. Rev.*, **137**, 4030–4046, doi:10.1175/2009MWR2880.1.

Sterk, H. A. M., G. J. Steeneveld, and A. A. M. Holtslag, 2013: The role of snow-surface coupling, radiation, and turbulent mixing in modeling a stable boundary layer over Arctic sea ice. *J. Geophys. Res.*, **118**, 1199–1217, doi:10.1002/jgrd.50158.

Tastula, E. M., T. Vihma, and E. L Andreas, 2012: Evaluation of Polar WRF from modeling the atmospheric boundary layer over Antarctic sea ice in autumn and winter. *Mon. Wea. Rev.*, **140**, 3919–3935, doi:10.1175/MWR-D-12-00016.1.

Tewari, M., and Coauthors, 2004: Implementation and verification of the unified Noah land surface model in the WRF model. *20th Conf. on Weather Analysis and Forecasting/16th Conf. on Numerical Weather Prediction*, Seattle, WA, Amer. Meteor. Soc., 14.2a. [Available online at https://ams.confex.com/ams/pdfpapers/69061.pdf.]

Valkonen, T., T. Vihma, M. M. Johansson, and J. Launiainen, 2014: Atmosphere–sea ice interaction in early summer in the Antarctic: Evaluation and challenges of a regional atmospheric model. *Quart. J. Roy. Meteor. Soc.*, **140**, 1536–1551, doi:10.1002/qj.2237.

Vázquez Becerra, G. E., and D. A. Grejner-Brzezinska, 2013: GPS-PWV estimation and validation with radiosonde data and numerical weather prediction model in Antarctica. *GPS Solutions*, **17** (1), 29–39, doi:10.1007/s10291-012-0258-8.